NATIONAL ADVISORY COMMITTEE FOR AERONAUTICS

TECHNICAL NOTE 2648

EXPERIMENTAL INVESTIGATION OF TRANSITION OF A MODEL HELICOPTER ROTOR FROM HOVERING TO VERTICAL AUTOROTATION

By S. E. Slaymaker, Robert R. Lynn,
and Robin B. Gray

Princeton University

NACA

Washington

March 1952

NATIONAL ADVISORY COMMITTEE FOR AERONAUTICS

TECHNICAL NOTE 2648

EXPERIMENTAL INVESTIGATION OF TRANSITION OF A MODEL HELICOPTER ROTOR FROM HOVERING TO VERTICAL AUTOROTATION

By S. E. Slaymaker, Robert R. Lynn,
and Robin B. Gray

SUMMARY

An experimental investigation has been carried out to study the variation of average induced flow around a model helicopter during transition from a hovering condition to steady autorotative vertical descent. Test data were obtained from simulated power failures under many different conditions. Results are summarized for variations in disk loading, blade angles, and rate of pitch change. Calculations were made of "effective induced velocity" for the various conditions. Sample comparisons of calculated and experimental performance were made.

The results of these tests show that the manner in which effective induced velocity varies during the transition to autorotation often differs greatly from the exponential variation assumed in the theoretical analysis (NACA TN 1907). It is also shown that conditions peculiar to vertical descent in the transition range cause variations in performance of the model not predicted by this method.

INTRODUCTION

This report covers one phase of an experimental program of model testing to study accelerated vertical flight of helicopters. This phase considers only the power-off vertical descent of a helicopter model during the first few seconds after power failure at a hovering condition.

In considering this transition from hovering flight to steady autorotation, one of the factors which must be known is the manner in which the induced flow of the rotor varies with time after power failure. Methods are well-known for calculation of initial and final values of average induced velocity (reference 1), but there has previously been neither theory nor empirical data to predict the manner in which the transition occurs between the two. In order to calculate performance

during transition, it has been assumed in reference 2 that average induced velocity v varies with time after power failure according to:

$$v = v_f - (v_o - v_f)e^{-kt}$$

where k is chosen arbitrarily. Testing the validity of this assumption has been the primary purpose of this phase of the model testing program.

This work was conducted at Princeton University under the sponsorship and with the financial aid of the National Advisory Committee for Aeronautics.

SYMBOLS

Physical quantities:

W	gross weight of helicopter, pounds
w	disk loading, pounds per square foot
b	number of blades per rotor
R	blade radius, feet
c	blade-section chord, feet
σ	rotor solidity ratio $\left(\frac{bc}{\pi R}\right)$
θ	blade-section pitch angle from zero lift, radians unless otherwise stated
ρ	mass density of air, slugs per cubic foot
t	time, seconds
t_θ	length of blade-pitch-change cycle, seconds
g	acceleration due to gravity $\left(32.2 \text{ ft/sec}^2\right)$

Velocities:

V	true airspeed of helicopter along flight path, feet per second

v	average effective induced velocity (including possible interference effects), feet per second (referred to herein as "induced velocity")
Ω	rotor angular velocity, radians per second
λ	inflow ratio (assuming v constant over disk)

Blade-section characteristics:

c_l	average section lift coefficient (at 0.75R)
a	slope of lift curve, per radian
c_{d_o}	section profile-drag coefficient
$\delta_0, \delta_1, \delta_2$	coefficients in power series for c_{d_o} as a function of angle of attack $\left(c_{d_o} = \delta_0 + \delta_1\alpha + \delta_2\alpha^2\right)$

Rotor characteristics:

T	rotor thrust, pounds
Q	rotor torque, pound-feet
C_T	rotor thrust coefficient $\left(\frac{T}{\pi\rho R^2(\Omega R)^2}\right)$
C_Q	rotor torque coefficient $\left(\frac{Q}{\pi\rho R^3(\Omega R)^2}\right)$

Subscripts:

o	initial value (for hovering)
f	final value (for steady vertical autorotative descent)

DESCRIPTION OF APPARATUS

Apparatus for this test program consisted of an enclosed drop tower, a model rotor system, and various units of electrical equipment for making and recording the necessary measurements.

The test tower (fig. 1) provides the necessary drop area, free from cross winds, weather, and so forth, having greater than 1-rotor-diameter clearance about the model in all positions. A control room above the test chamber houses all drive equipment and measuring apparatus. A guide wire down the center of the tower keeps the fall of the model truly vertical. The model can be pulled up into the control room to make necessary adjustments before each drop test.

The first test model (fig. 2) consisted of a rigid, controllable-pitch rotor system having the following characteristics:

Rotor diameter, ft	6
Number of blades	2
Solidity ratio	0.07
Blade section (no twist or taper)	NACA 0015
Rotor inertia (about center rotation), slug-ft^2	0.1865
Dry weight, lb	5.6

Blade pitch changes up to 10° could be made after power failure by means of a hydraulic actuator which was adjustable for various rates of pitch change. Completion of the pitch-change cycle was signalled by lighting of a photoflash bulb (fig. 2). The start of the test was signalled by another flash bulb on the drive shaft which was triggered by the model release mechanism. The guide wire passed through the axis of the model and the wire contact bushings were spaced widely enough to prevent appreciable tipping of the model axis from the vertical.

Additional tests were also made with a second larger model in order to investigate possible scale effects (fig. 3). Characteristics of this model were as follows:

Rotor diameter, ft	8
Number of blades	2
Solidity ratio	0.08
Blade section (no twist or taper)	NACA 0015
Rotor inertia, slug-ft^2	0.660
Dry weight, lb	12.3

Operation of this model was similar to the other except that a number of flash bulbs were on the model to record each 2° pitch change, thus enabling a true curve to be obtained of blade pitch variation with time during the pitch-change cycle.

During a drop test, all data were taken by photoelectric tubes with appropriate amplifying circuits and were recorded against a time base by a Heiland recording oscillograph. Vertical position of the model was recorded by means of horizontal light beams and phototubes along the drop

path. Rotor speed was counted throughout the drop by a vertical light beam passing through the rotor to a phototube on the ceiling. Another tube picked up signals from the photoflash bulbs to record the start of the drop and pitch-change data.

In order that basic model characteristics might be known for the range of Reynolds numbers covered in these tests, a static-thrust test stand was built. Measurements of thrust and torque were made on the models at various rotor speeds and blade angles in order to calculate rotor coefficients and average blade-section coefficients.

TEST PROCEDURE

A typical test was begun by setting the desired initial blade pitch angle for hovering and also the amount of pitch reduction after release. Time of pitch change was set approximately by adjusting the needle valve on the pitch-control mechanism. With flash bulbs installed in the model and the release mechanism (fig. 4), the model was lowered to starting position on the end of the drive shaft (fig. 5). With the tower darkened except for phototube light beams, the model was started whirling and brought to about 90-percent hovering speed. The oscillograph record was then started and the model speed was gradually increased to hovering. As the model started to lift, it released automatically from the drive shaft and simultaneously the pitch reduction began. The oscillograph was kept running to record data from the phototubes until the model hit the shock absorber at the bottom of the tower. From the developed record, graphs were plotted of position, blade pitch, and rotor speed against time for each test. For the 6-foot rotor, blade pitch was assumed to be a straight-line variation with time during the pitch-change cycle. Curves of descending velocity and acceleration against time were then calculated by differentiation of the displacement curve. Finally, a curve of average induced velocity against time was computed, using the following formula from reference 2:

$$v = V + \frac{4(\dot{V} - g)W}{\Omega\rho abcgR^2} - \frac{2R\theta\Omega}{3}$$

The range of test conditions covered by the two models included variations in disk loading from 0.2 pound per square foot to 1.1 pounds per square foot with corresponding Reynolds numbers from 300,000 to 800,000. Hovering values of θ varied from 6° to 12° and autorotative values of θ ranged from 0° to 4°. Pitch-change intervals t_θ varied from about 0.1 second to 3.0 seconds. For each set of test conditions at least two drops were made to be sure that results were reproducible within the limits of experimental error.

PRECISION

Since accelerations must be obtained by double differentiation of displacement data, a high order of accuracy is required for all measurements. Hence, electronic recording of all data was used in order to eliminate appreciable time errors of observation. The accuracy of the results then rested primarily on accuracy in reading oscillograph records and also on accuracy of measurement in determining phototube positions.

By conservative estimate, time at any position could be read on the oscillograph record to the nearest 0.005 second and measurement error between any two phototubes has been determined by several measurements to be not over 3/32 inch. On this basis, velocity curves were obtained with accuracy, better than ±3 percent up to 16 feet per second, and they are still within ±6 percent at 30 feet per second. Calculation of acceleration accuracy was based on the premise that a velocity curve must be a smooth curve within its limits of accuracy. This gives error limits varying from less than 5 percent in the high acceleration range to more than 100 percent for very low accelerations. However, in most cases this is an approximately constant error of ±1.5 feet per second per second. Since acceleration enters the calculation of induced velocity in the form $(\dot{V} - g)$, the errors in $\dot{V}$ obviously have a much smaller effect on the value obtained for average induced velocity.

Also required for calculation of induced velocity are rotor-speed and blade-angle data. Rotor-speed accuracy is ±2 percent, based on an estimated time reading error of 0.003 second in 2 revolutions. Calibration of the blade-pitch-change mechanism of the 6-foot model showed straight-line variation of blade pitch with time for changes up to 7°, with less than 5-percent error for an 8° pitch change.

As a result of the various degrees of accuracy mentioned above, the curves of average induced velocity have a calculated accuracy of better than ±7 percent in most cases. Limits of accuracy of various curves are illustrated for a sample case in figure 6.

In addition to errors in data recording and reduction, other inaccuracies are possible in the tests themselves. Friction between the model and the guide wire is a possible source of error, but there has been no evidence that it was appreciable except in a few cases where vibration occurred during the drop. In these instances the test results were erratic and hence were discarded. Normally, two tests under the same conditions would duplicate each other within plotting accuracy. As an extra check, the acceleration due to gravity was checked within 3 percent by dropping the model hub down the wire without blades.

Errors in rotor speed occasionally occurred through erratic operation of the release mechanism. However, the addition of a booster spring to the mechanism practically eliminated this trouble. Also, the correct rotor speed for hovering was known from static-thrust data so that any tests whose records showed marked errors in release speed could be discarded.

RESULTS AND DISCUSSION

Test Results

Data resulting from a typical test are shown in graph form in figure 7. Displacement and rotor-speed data are plotted for the particular conditions of disk loading, blade angles, and rate of pitch change of this test. Also, the average-induced-velocity curve computed from these data is shown in the same figure.

The effects of changes in rate of pitch change on test results of a particular model configuration are illustrated in figures 8 and 9. A family of displacement and rotor-speed curves are shown in figure 8 for different pitch-change rates and figure 9 shows the resulting family of computed curves of average induced velocity.

Effects of changes in disk loading on test results are illustrated in figure 10, where other parameters are held constant. Comparative values of average induced velocity may be noted in figure 9 for low and high disk loadings.

The great mass of data from all the tests of this program has been summarized in figure 11. It has been found that when the test results are plotted in Glauert's coefficients (1/f against 1/F), the most significant variable is rate of pitch change. Hence, figure 11 represents a family of curves for different pitch-change rates for all the tests of both models. It is interesting to note that, as the length of pitch-change interval increases, the shape of the curve seems to approach the results of recent experiments for steady-state power-on vertical descent from hovering to steady autorotation (reference 3).

Computed Results

It is apparent from inspection of figures 12 and 13 that the test results are not in very good agreement with performance curves computed for the test conditions by the method of reference 2. This is believed to be primarily due to the unexpectedly high values of descending velocity

which were encountered experimentally. The causes of these high rates of descent, which will be discussed in detail below, were not included in the analytical method used to compute the performance curves.

In reference 2 an exponential variation of average induced velocity with time was arbitrarily assumed for lack of better information. It now appears from the experimental results that this assumption could be improved upon, particularly for the case of rather high rates of blade pitch change. It may be noted from figures 12 and 13 that, when the pitch change is rapid, the induced-velocity curve takes a sudden dip and then rises to a value higher than that of the assumed exponential curve. When slower pitch change is used, the agreement seems to be better.

High Descending Velocities

A source of considerable difficulty in analyzing test results was the fact that both models appeared to reach much higher rates of autorotative descent than were predicted by the Glauert empirical curves. Calculated rates of autorotation for both models were best approximated by the formula $V = 28\sqrt{w}$ and, for disk loadings less than about 0.5 pound per square foot, the models should stabilize at this rate within the drop height of the tower. However, it was soon noted that even the lightest models were reaching rates of descent much higher than this at the bottom of the tower and heavier ones were still accelerating. Estimated autorotative rates of descent from test data came to about $V = 37\sqrt{w}$. This led to considerable speculation as to possible scale effects and interference effects of the tower enclosure, but it was later determined experimentally that the models would stabilize at normal rates of autorotative descent when released from a condition of zero thrust at autorotative speed instead of a hovering condition. Under such conditions they checked Glauert's data within a few percent.

It was therefore apparent that initial conditions are important in determining performance in the transition range. To explore this effect further, a series of tests were made with different initial conditions. Starting thrusts from 0 to 161 percent of hovering were used, with a rapid pitch change and 0° blade pitch for the final angle in each case. Rotor speed and disk loading were constant for all tests. Results are plotted in figure 14 and show plainly the wide range of final values obtained. It seems obvious that the model was being strongly accelerated by falling into its own downwash, however, no corrections were made to the data for this effect, as a similar condition exists for a full-scale helicopter during the initial part of its transition to autorotation.

A test of flow persistence in the downwash area was made with a hot-wire anemometer system. The model was turned at hovering thrust at its starting position in the tower. The blade angle was then instantly reduced to 0° without dropping the model and the downwash velocity was

recorded. It was found that it required 2 to 3 seconds after the blade pitch changed to zero for the velocity at any point to fall to half its initial value and about 20 seconds passed before it became undetectable. Since the average drop test of the model was less than 3 seconds, the flow persistence was easily great enough to have a strong effect. Furthermore, the flow test conditions were probably overly severe for, when blade pitch is reduced to zero without dropping the model, it should act as a brake to the flow, whereas it would probably have much less braking effect when dropped.

In an effort to explore this effect further, a special small, light model was made (rotor diam., 4 ft; disk loading, 0.07 pound per square foot), with the objective of covering a greater portion of the transition period within the drop distance available in the test tower. Velocity curves for this model when released from initial conditions of hovering and zero thrust are shown in figure 15. It is seen here that model descending velocity, when the initial condition is hovering, peaks at an abnormally high value and then falls back towards a final steady-state value. However, it appears that more than twice the time will be required to stabilize than when the model is released from a zero-thrust condition.

Recirculation Effects

It seemed possible that the high descending velocity effects noted above might be due largely to recirculation of air within the tower. Hence, a rather thorough survey was made of air patterns in the tower. Figure 16 summarizes results obtained by a smoke wand and also by a hot-wire anemometer. The smoke survey showed clearly the general pattern of a strong slipstream and a large turbulent area outside it. Air velocities were surprisingly low in the upper and outer part of the space. The anemometer survey gives air velocity values for the 8-foot model hovering at a disk loading of 0.5 pound per square foot. Curves are plotted along a radius at various distances beneath the rotor, with downward displacement of the curve for downward air velocity. Note that downward velocity is very high beneath the rotor, but net upward velocity near the walls is very low. It is believed that, because of the low net upward velocity outside the slipstream and also the large turbulent area, the recirculation energy of the air must be negligible.

Scale Effects

In evaluating the results of this test program, consideration of possible scale effects must be included. Tests were made in the range of Reynolds numbers from about 300,000 to 800,000, so that caution should be used in any extrapolation of these results to full-size rotors. However, it is encouraging that steady autorotation descending velocities

of both models checked Glauert's data closely, since these are said to agree fairly well with full-scale test performance. Also, no appreciable differences were found between the two models when results were plotted as curves of $1/f$ against $1/F$ (fig. 11).

The usual Reynolds number corrections have been made through static-thrust testing of the models in the test range and using coefficients thus obtained for all calculations. Details of this process are presented in the appendix. There is evidence that test data such as these may be best extrapolated to full scale by use of Froude numbers, but such results are not at present available.

CONCLUSIONS

From an experimental investigation of the variation of average induced flow of a model helicopter during transition from hovering flight to steady autorotative vertical descent, the following conclusions may be drawn:

1. The experimental data indicate that the exponential variation of average induced velocity with time which was assumed in NACA TN 1907 does not permit reasonable accuracy to be achieved in computing the transient motion of a helicopter between the hovering state and steady vertical autorotation. Especially required is consideration of the accelerating effect of the rotor slipstream in which the helicopter is descending. A more realistic shape must be assumed for the induced-velocity curve, particularly in the case of rapid reduction of blade pitch angle.

2. Good agreement of model performance with computed values may be obtained for steady-state conditions when known coefficients for the actual Reynolds number are used.

3. While loss of altitude at a given time after power failure can be lessened by reducing blade pitch slowly, a rapid pitch change appears more desirable in order to minimize loss of rotor speed.

Princeton University
Princeton, N. J., Dec. 9, 1949

APPENDIX

STATIC-THRUST ANALYSIS OF MODELS

Slope of lift curve a.- Figures 17 to 19 show the thrust-torque test-stand results of the test models. Measurements of thrust and torque were made at various blade angles and rotor speeds with the stand so located that at least 1-rotor-diameter clearance existed in all directions.

Data thus obtained were found to be in good agreement with a value for a of 5.75 per radian which was obtained by other investigators for similar blades at corresponding Reynolds numbers (reference 4).

Drag polar coefficients δ_0 and δ_2.- Values for δ_0 were obtained by measurements of torque at zero lift at various rotor speeds. Results are plotted in figure 17 as $\left(c_{d_o}\right)_{min}$ against Reynolds number (at 0.75R).

Figure 19 is a plot of C_T against C_Q calculated from faired experimental curves. Corresponding values of c_l and c_d were calculated from the following equations which have been derived from blade element theory:

$$c_l = \frac{6C_T}{\sigma}$$

$$c_d = \frac{8}{\sigma}\left(C_Q - C_T\lambda\right)$$

$$\lambda = \frac{2}{3}\theta - \frac{4C_T}{a\sigma}$$

It was found that, for all Reynolds numbers measured, the drag polar (see fig. 18) could be expressed as:

$$c_d = \left(c_{d_o}\right)_{min} + 0.9\alpha^2$$

Accuracy.- The accuracy of the data for C_T plotted against C_Q (fig. 19) was estimated to be within 7 percent, based on a measurement error of 2 percent in rotor speed, 3 percent in thrust, and 2 percent in torque.

The accuracy of the data for $(c_{d_o})_{min}$ plotted against Reynolds number (fig. 17) was estimated to be approximately 2 percent, since errors in torque and rotor speed were less at zero lift.

The drag polar resulting agrees with other similar investigations (reference 4).

REFERENCES

1. Nikolsky, A. A., and Seckel, Edward: An Analytical Study of the Steady Vertical Descent in Autorotation of Single-Rotor Helicopters. NACA TN 1906, 1949.

2. Nikolsky, A. A., and Seckel, Edward: An Analysis of the Transition of a Helicopter from Hovering to Steady Autorotative Vertical Descent. NACA TN 1907, 1949.

3. Castles, Walter, Jr., and Gray, Robin B.: Empirical Relation between Induced Velocity, Thrust, and Rate of Descent of a Helicopter Rotor as Determined by Wind-Tunnel Tests on Four Model Rotors. NACA TN 2474, 1951.

4. Knight, Montgomery, and Hefner, Ralph A.: Static Thrust Analysis of the Lifting Airscrew. NACA TN 626, 1937.

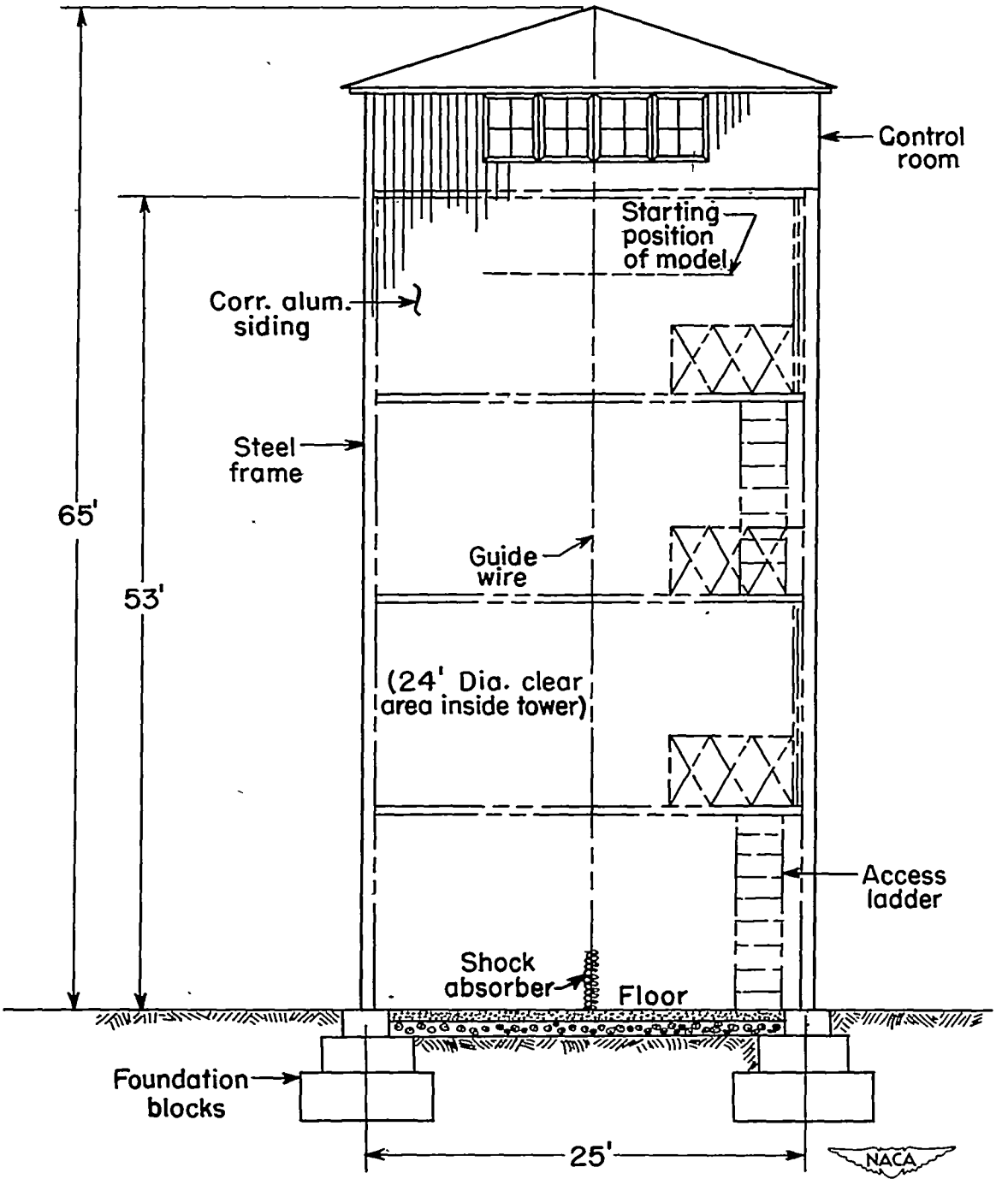

Figure 1.- Helicopter model research tower.

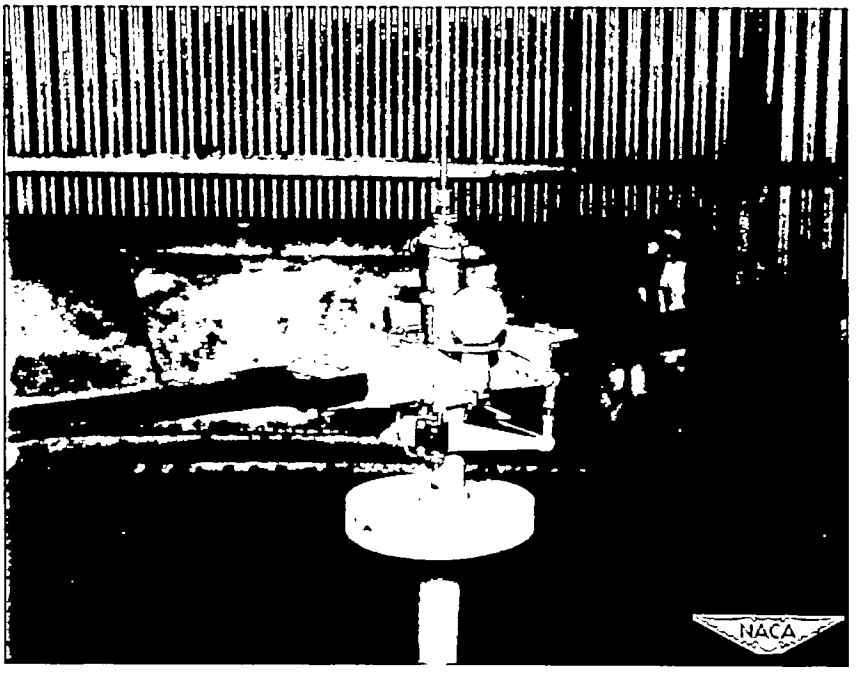

Figure 2.- Hub mechanism of 6-foot model helicopter. Note photoflash bulb with electric contacts on blade pitch cross arm. Batteries and pitch-control needle valve are on far side. Lead weight on bottom is for $w = 0.5$.

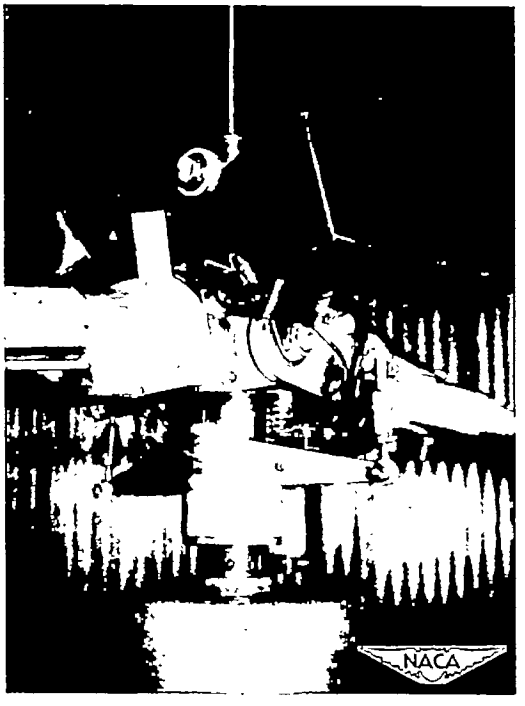

Figure 3.- The 8-foot model used for tests at higher Reynolds numbers.

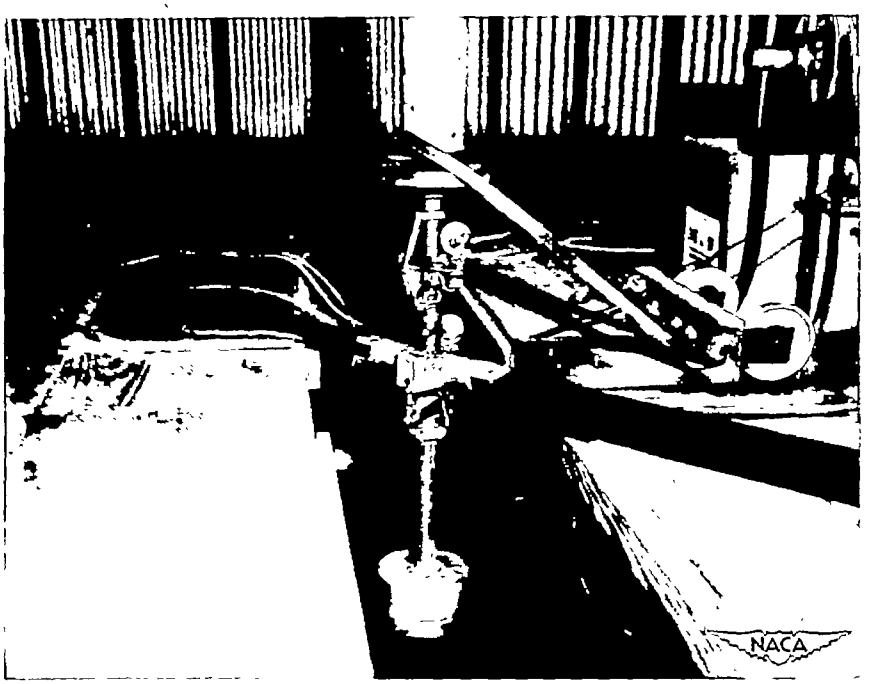

Figure 4.- View showing model attached to release mechanism before being lowered to starting position.

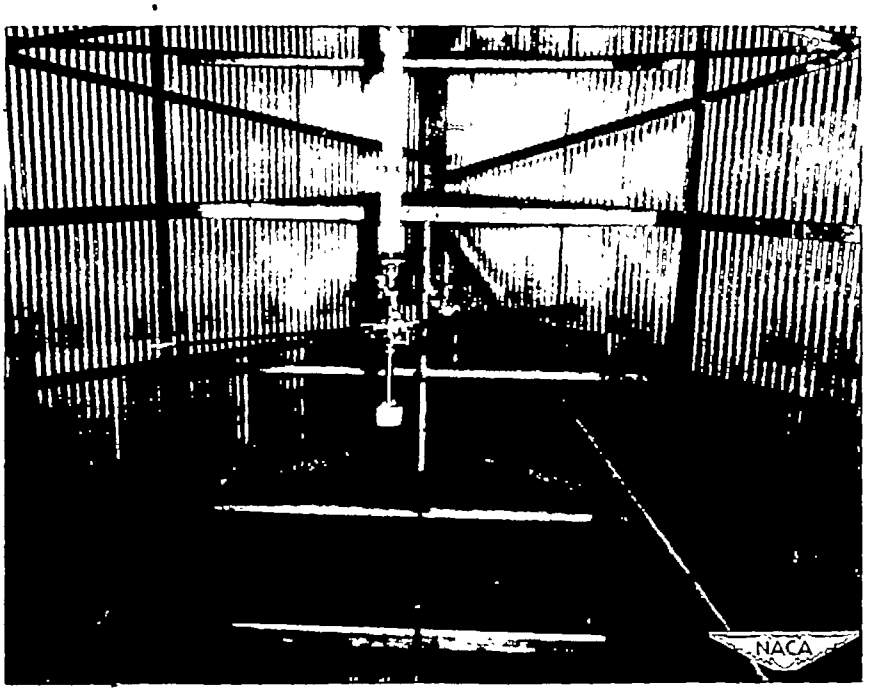

Figure 5.- Model on drive shaft in starting position. Weights shown are for $w = 0.1$. Note phototubes on far side of tower.

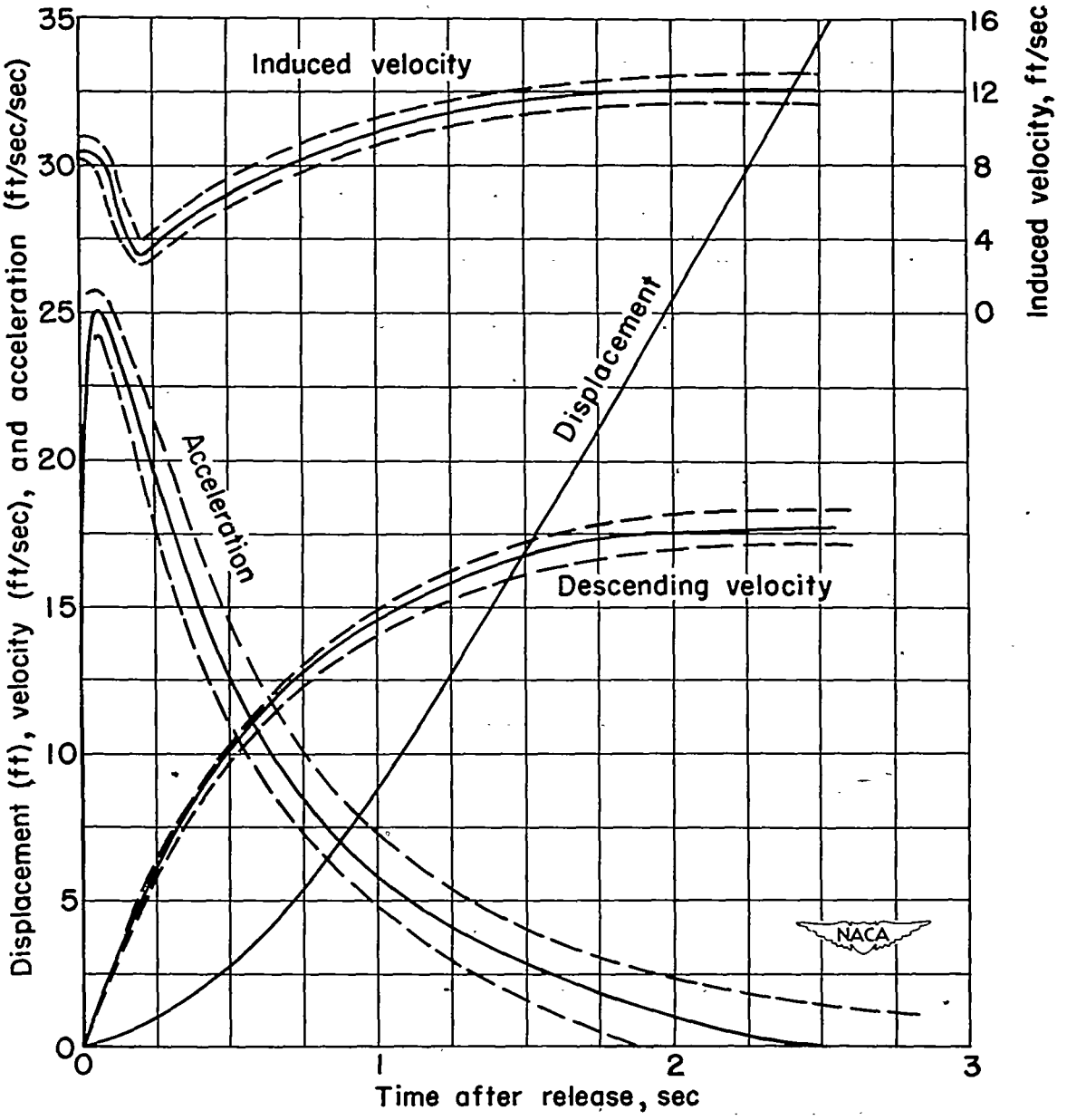

Figure 6.- Calculated limits of accuracy of velocity, acceleration, and induced-velocity curves worked out for a sample case. $w = 0.2$; $\theta_o = 8\frac{1}{4}^\circ$; $\theta_f = 0^\circ$; $t_\theta = 0.2$ second.

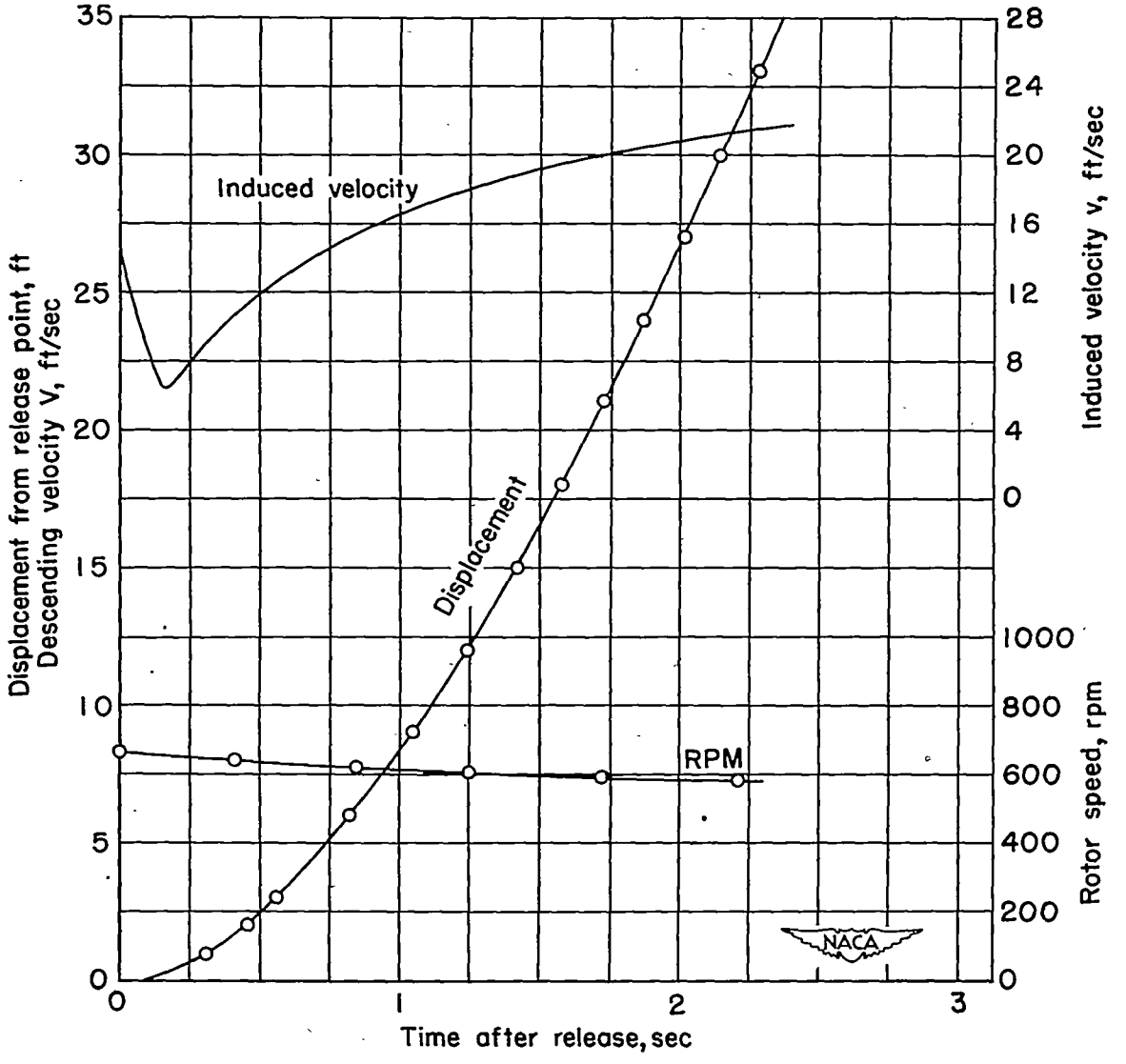

Figure 7.- Sample plot of induced-velocity variation with time and plots of experimental data from which it was calculated. $w = 0.5$; $\theta_o = 10^\circ$; $\theta_f = 4^\circ$; $t_\theta = 0.09$ second; $\rho = 0.00245$ slug per cubic foot.

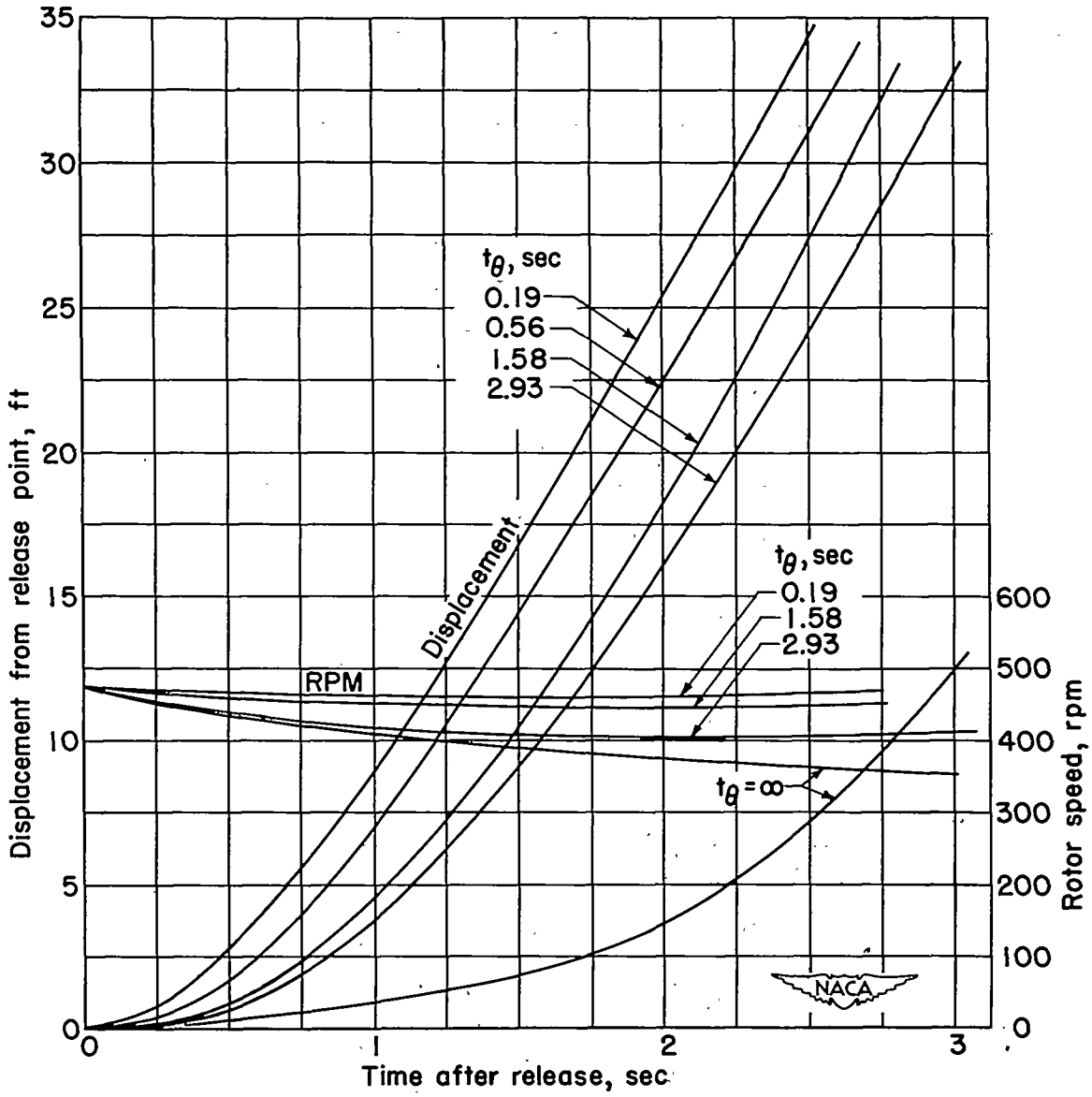

Figure 8.- Effect of variation in t_θ on displacement and rotor speed.

$w = 0.2$; $\theta_o = 8\frac{1}{4}^\circ$; $\theta_f = 0^\circ$.

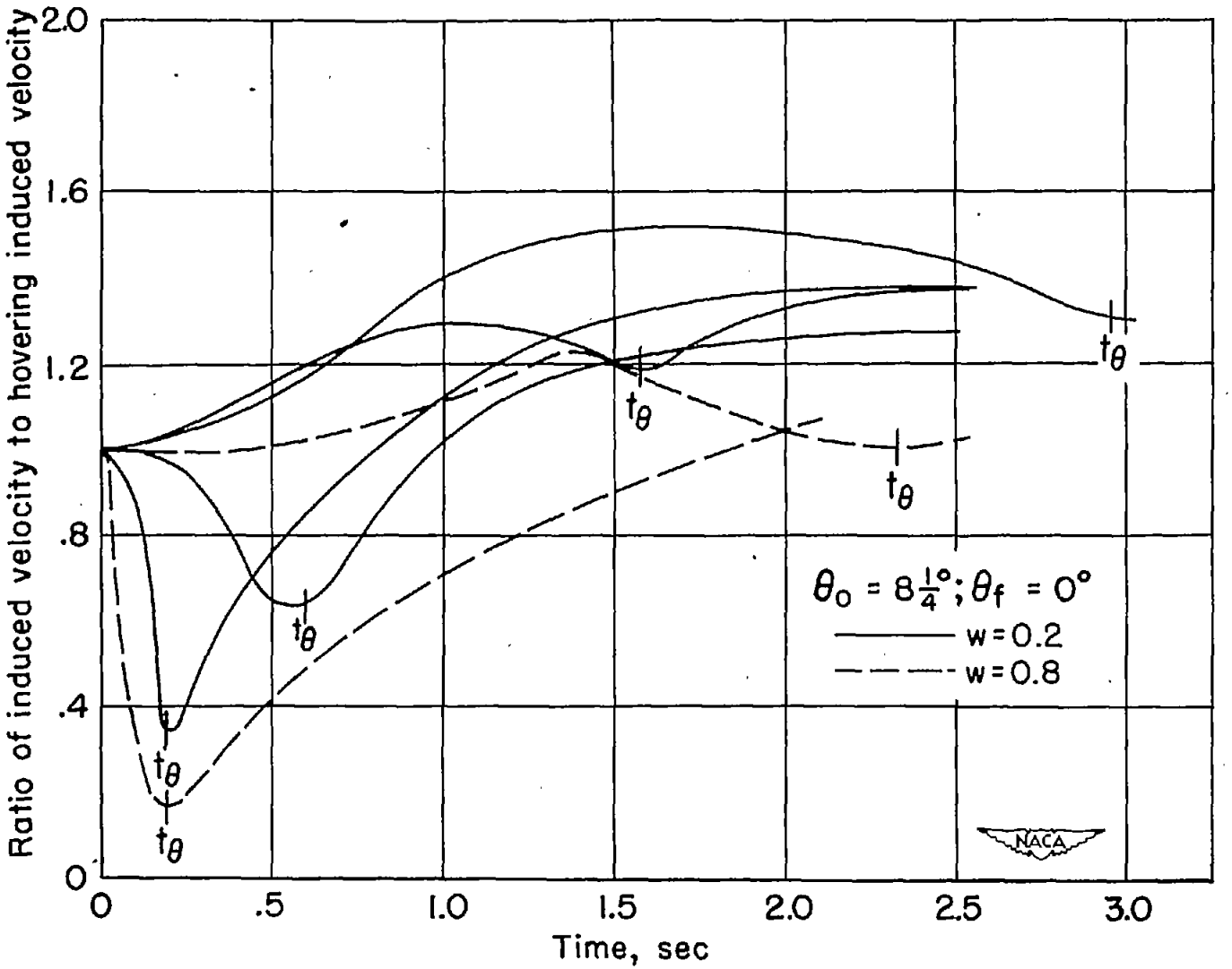

Figure 9.- Effect of variation in t_θ on induced-velocity ratio for the 6-foot model.

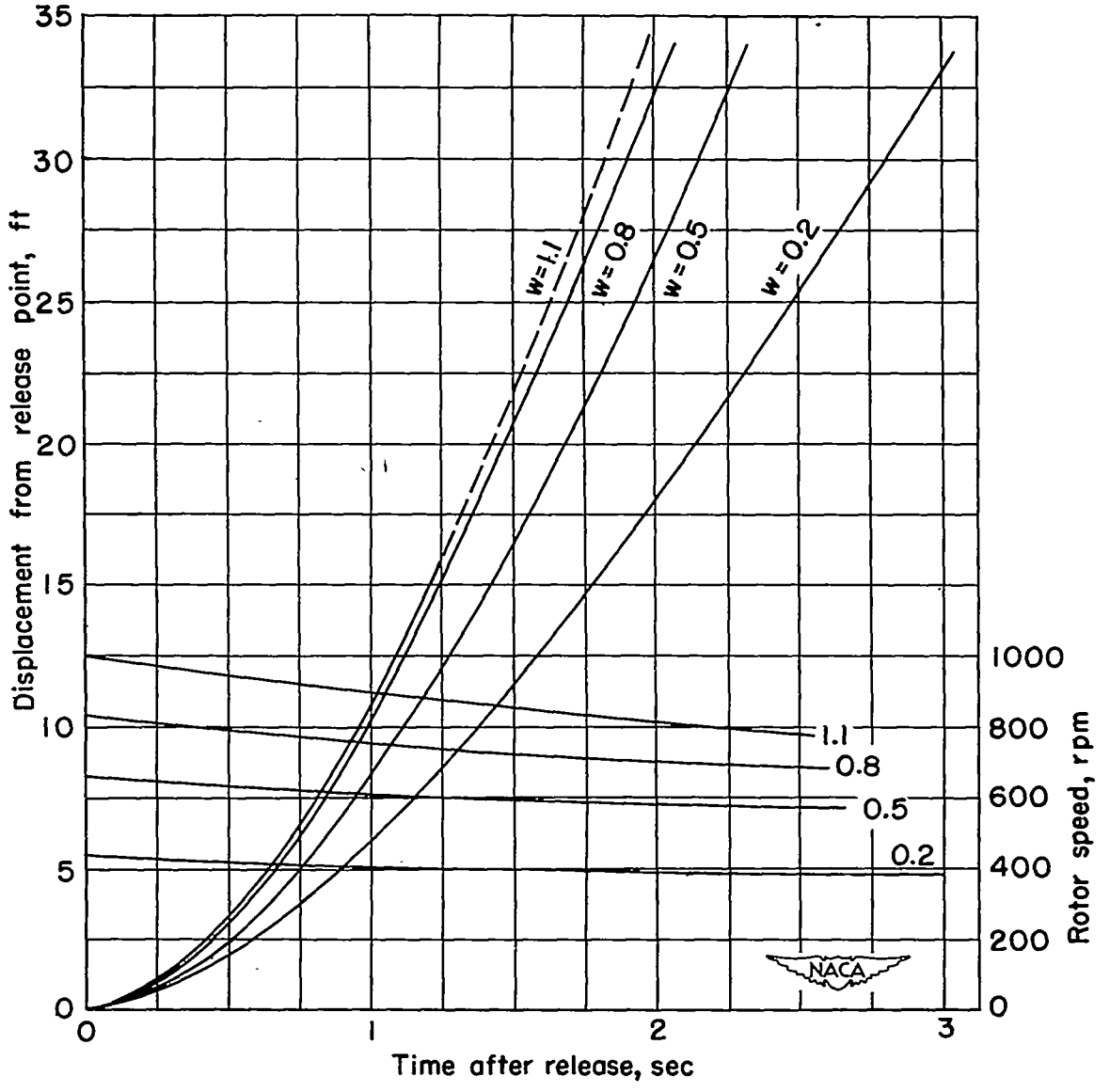

Figure 10.- Effect of change in disk loading on displacement and rotor-speed curves. $\theta_o = 10^o$; $\theta_f = 4^o$; $t_\theta \approx 0.1$ second.

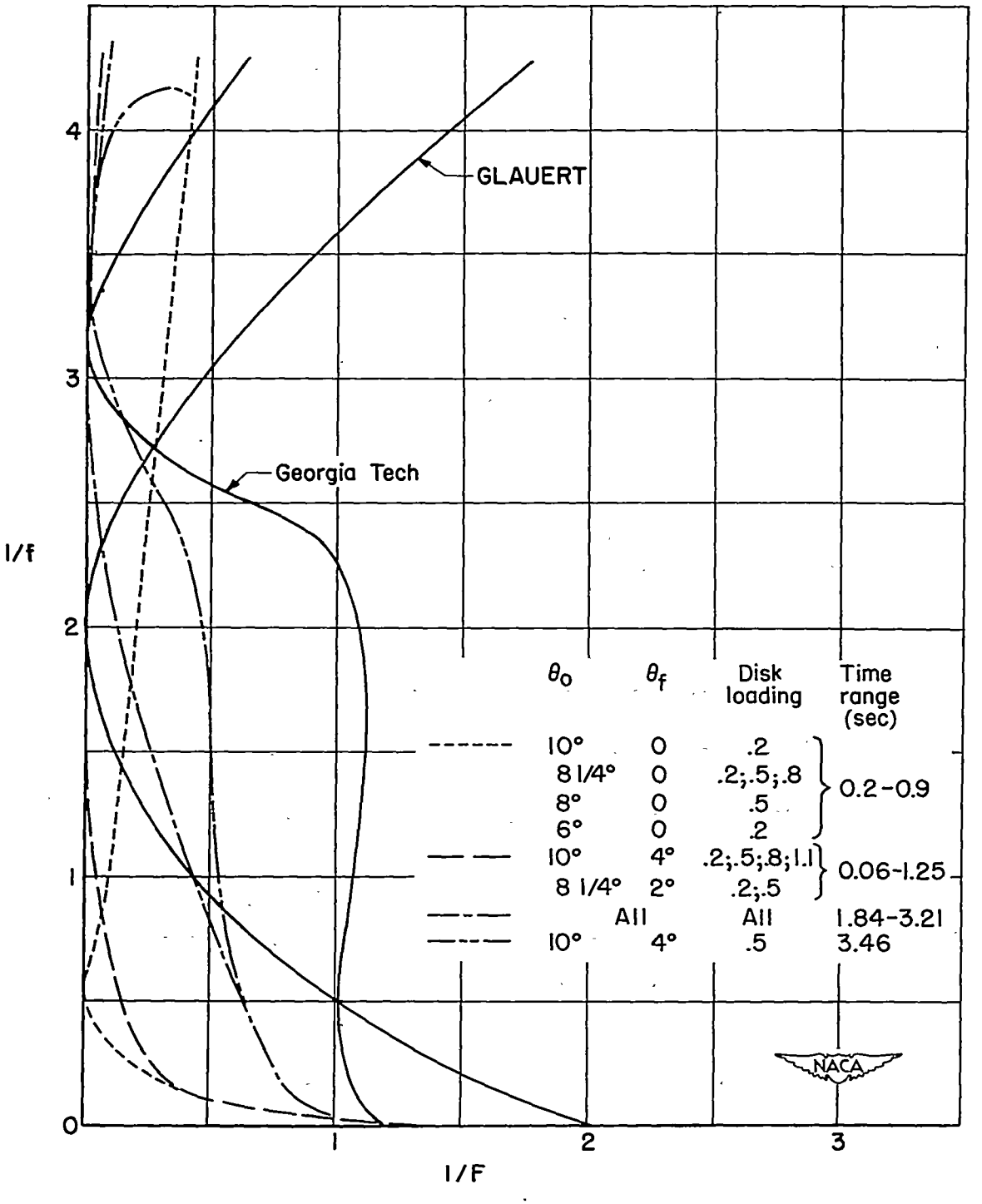

Figure 11.- Plot of $\frac{1}{f}$ against $\frac{1}{F}$ based on hovering thrust.

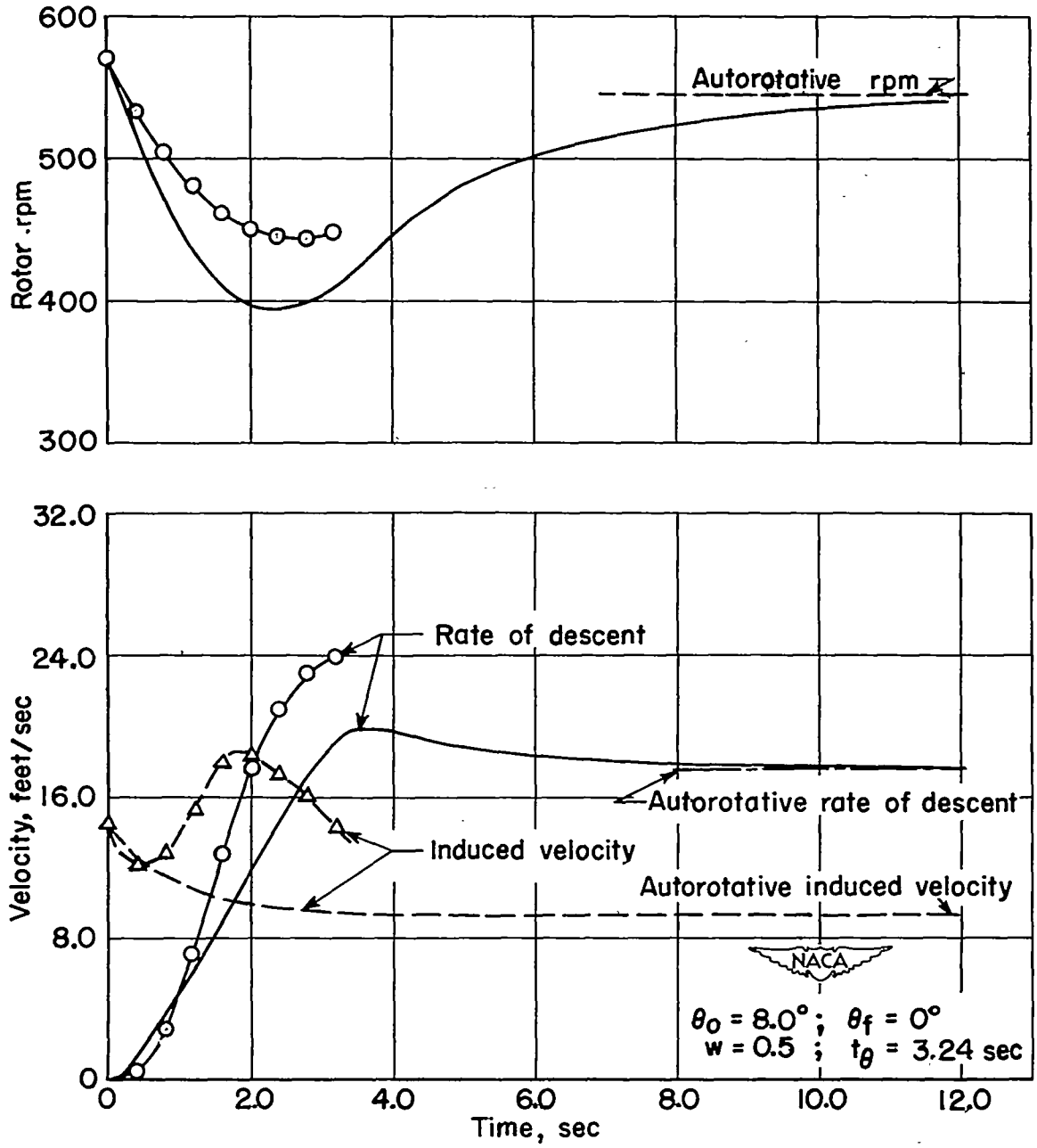

Figure 12.- Theoretical and experimental comparison for slow pitch change. Exponential variation of induced velocity assumed for theoretical data.

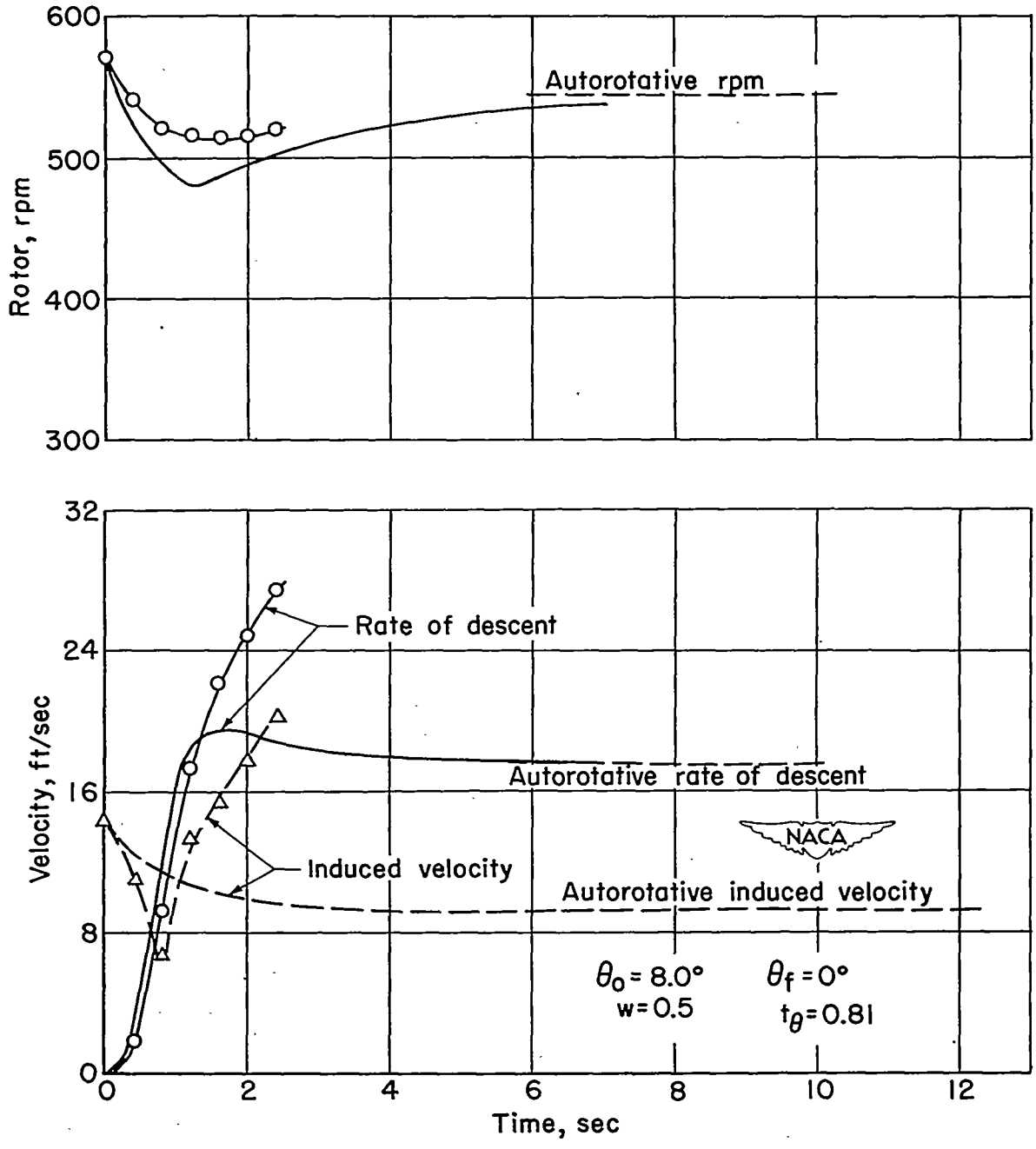

Figure 13.- Theoretical and experimental comparison for fast pitch change. Exponential variation of induced velocity assumed for theoretical data.

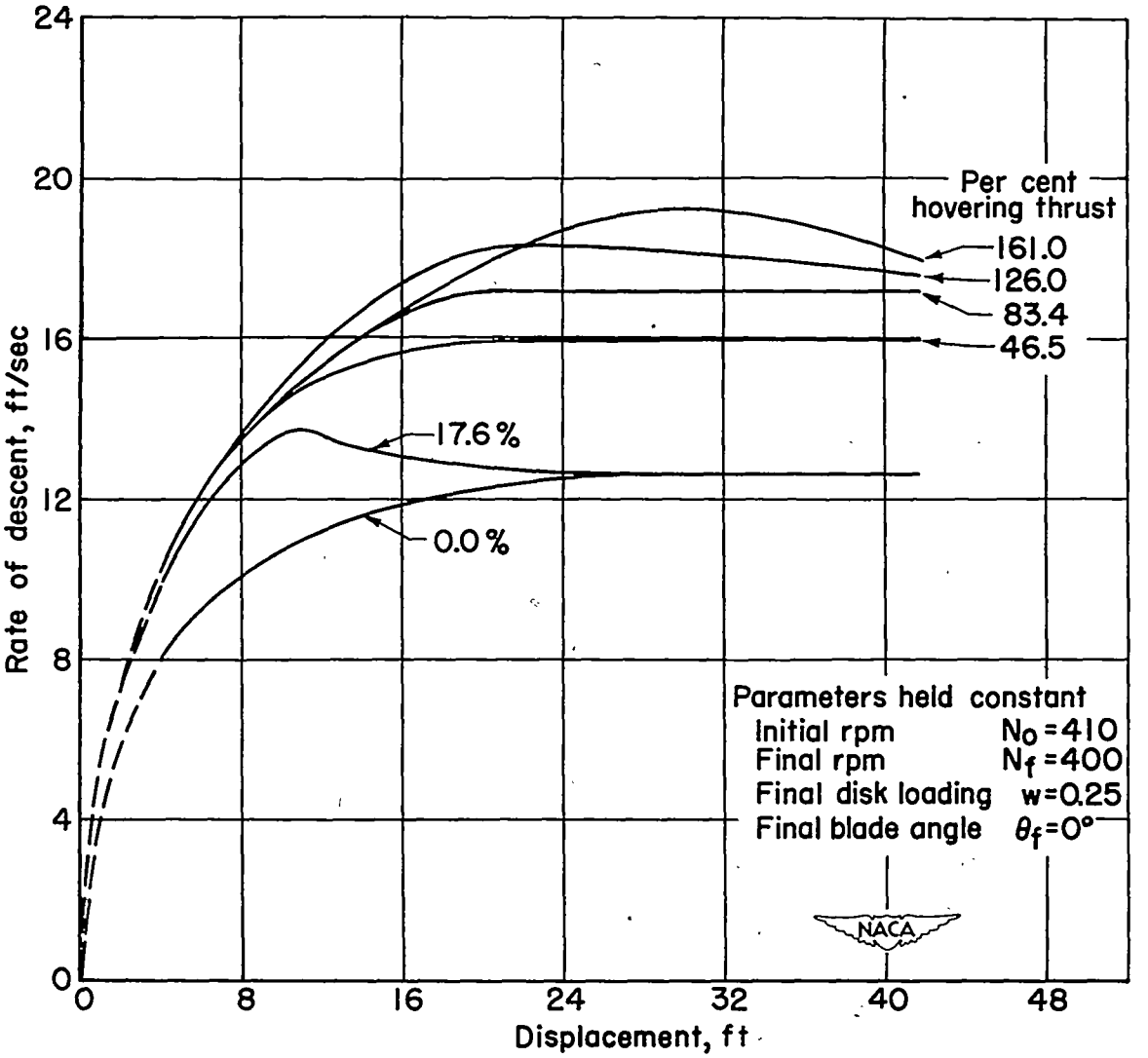

Figure 14.- Effect of initial thrust on descending velocity.

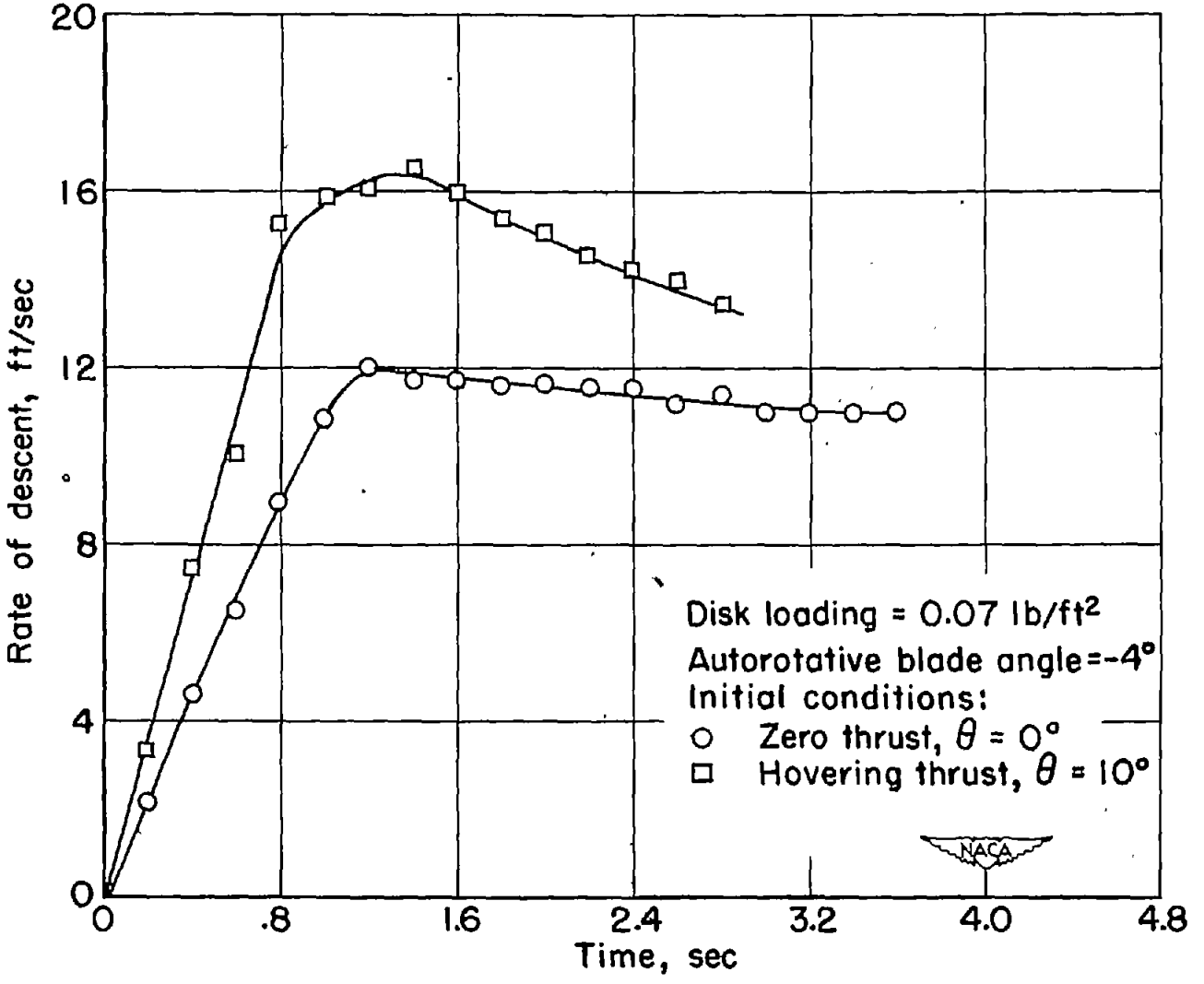

Figure 15.- Effect of initial conditions on descending velocity during transition to autorotative vertical descent for special small model.

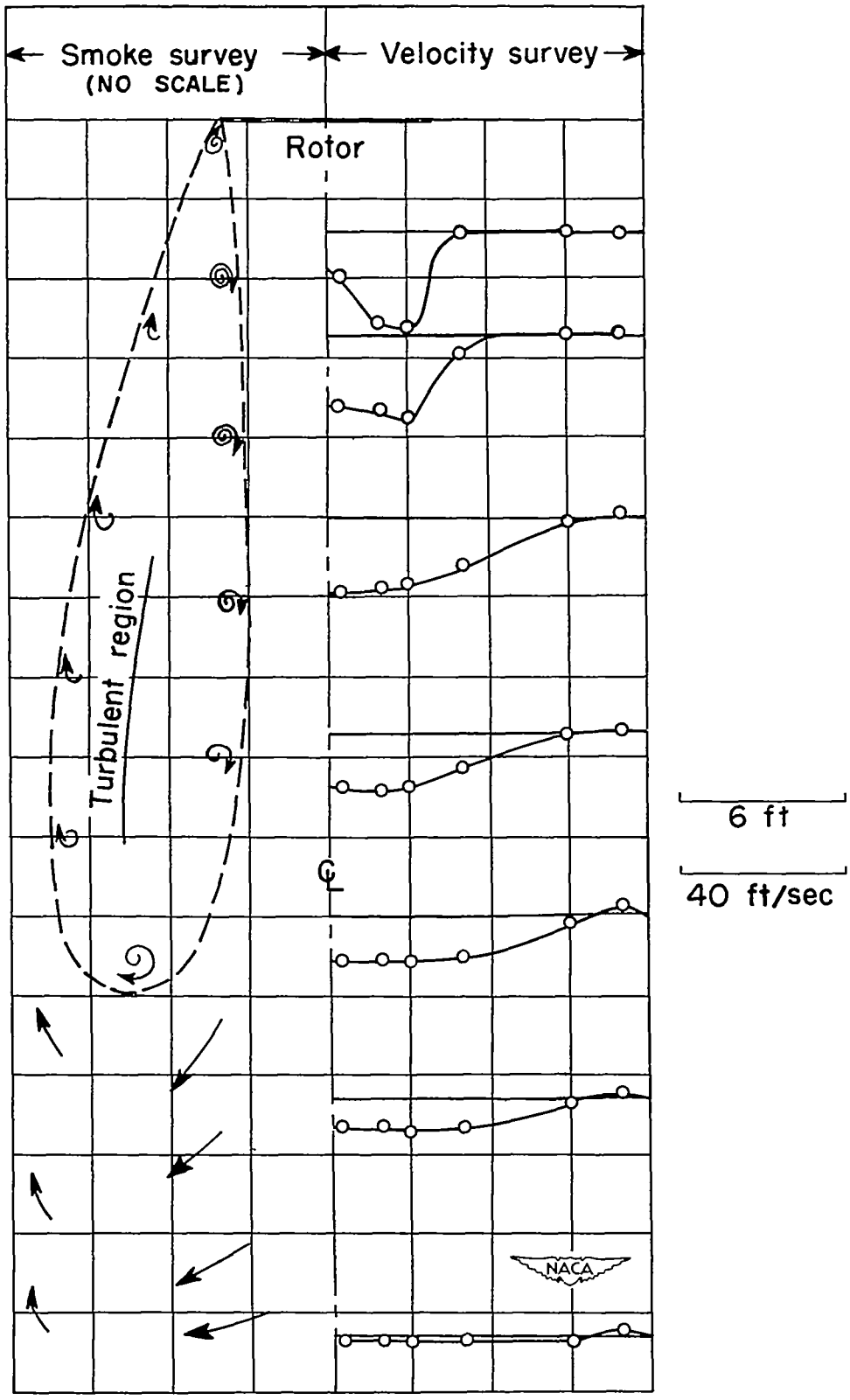

Figure 16.- Velocity survey and smoke survey of tower for 8-foot model. w = 0.5 pound per square foot.

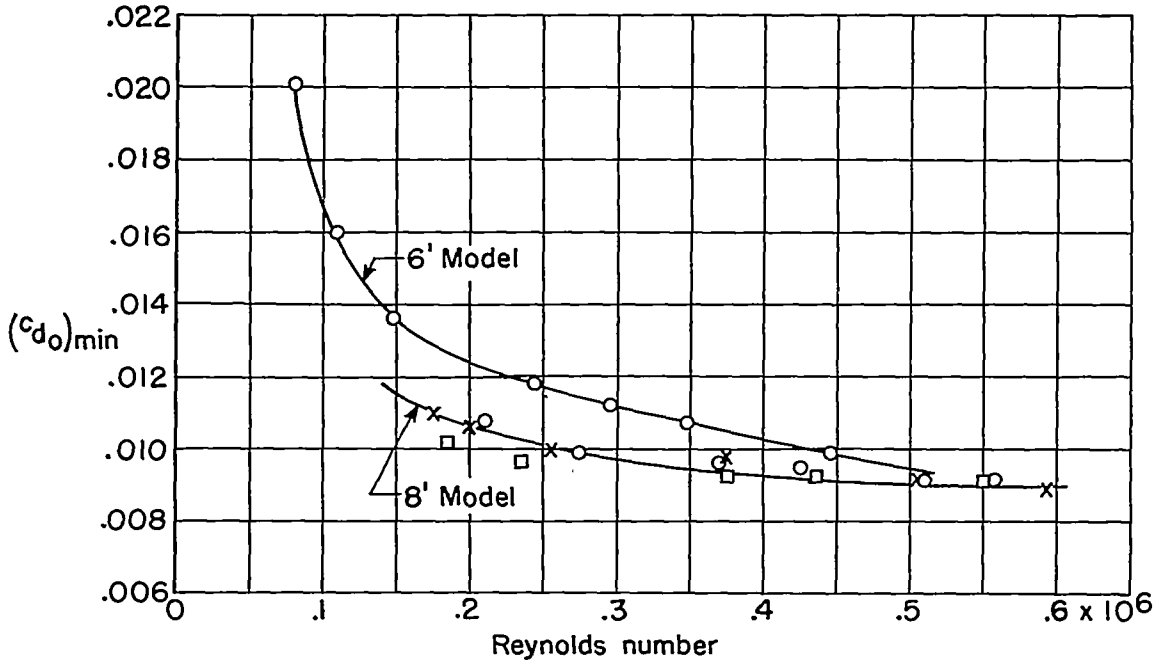

Figure 17.- Average minimum profile-drag coefficient (0.75R) calculated from static-thrust analysis of model.

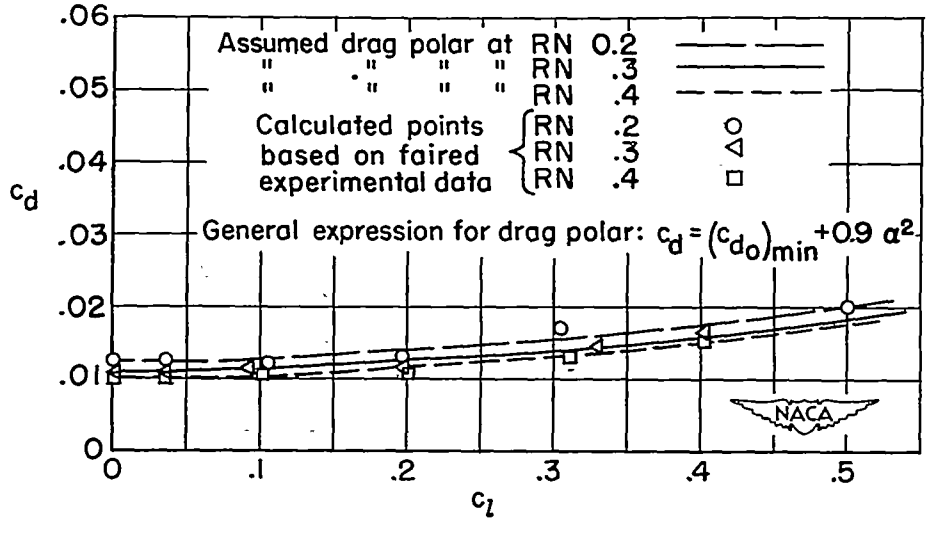

Figure 18.- Blade-section characteristics for various Reynolds numbers $(\times 10^6)$ determined from static-thrust analysis.

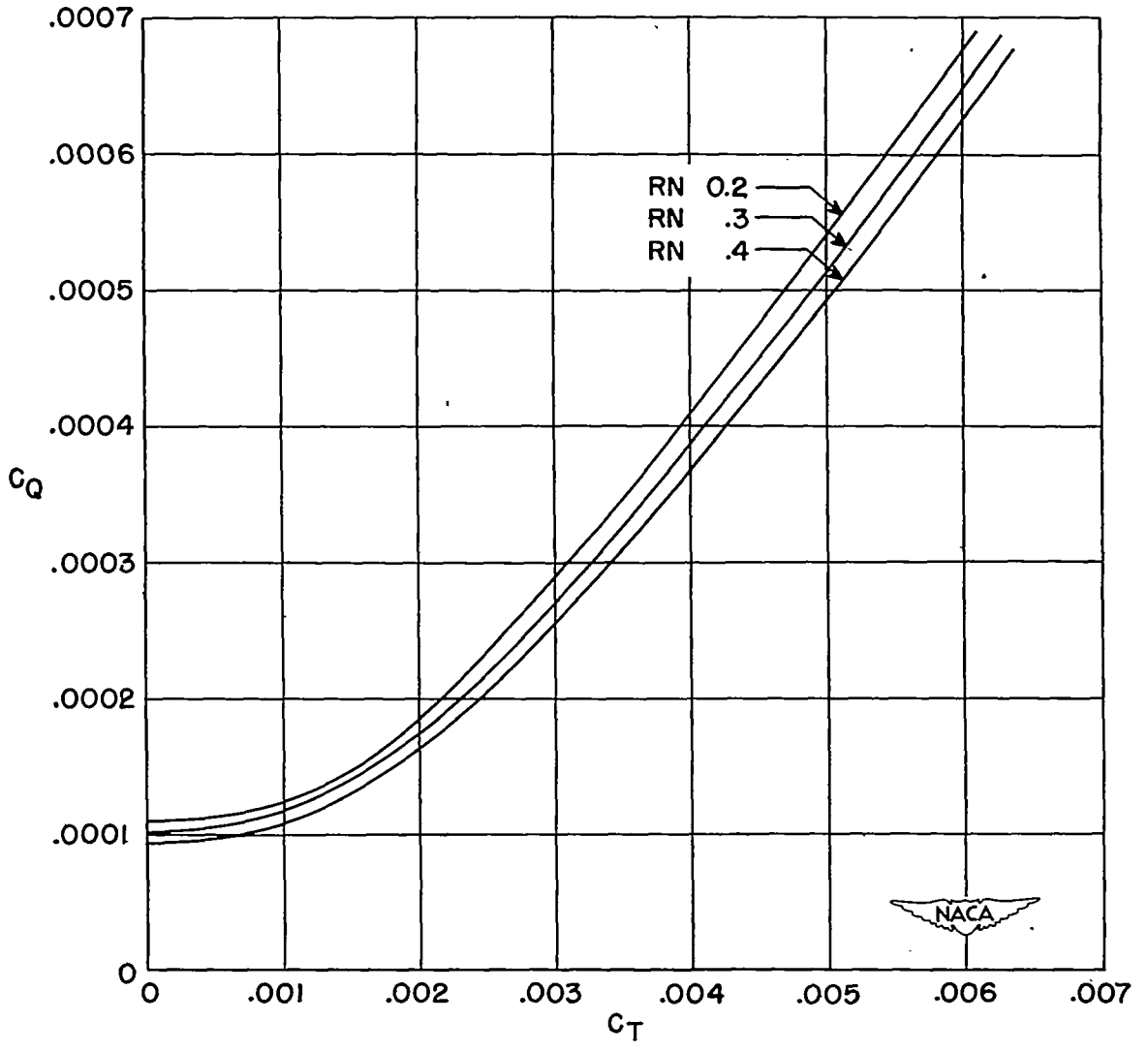

Figure 19.- Model rotor characteristics at various Reynolds numbers $(\times 10^6)$ prepared from faired static-thrust-analysis data.

NACA-Langley - 3-11-52 - 1000